Formation of Molecular Bromine from the Reaction of Ozone with Deliquesced NaBr Aerosol: Evidence for Interface Chemistry

S. W. Hunt, M. Roeselová,† W. Wang, L. M. Wingen, E. M. Knipping,‡ D. J. Tobias,* D. Dabdub,§ and B. J. Finlayson-Pitts*

Department of Chemistry, University of California, Irvine, California 92697-2025

Received: July 22, 2004; In Final Form: September 28, 2004

The reaction of ozone with aqueous sodium bromide particles is investigated with a combination of aerosol chamber experiments, kinetics modeling, and molecular dynamics simulations. The molecular bromine production in the chamber experiments is approximately an order of magnitude greater than that predicted by known chemistry in the gas and bulk aqueous phases with use of a comprehensive computer kinetics model. Molecular dynamics simulations indicate that ozone has significant residence time at the air−solution interface, while making frequent contacts with bromide ions for as long as 50 ps in the surface layer of a 6.1 M NaBr solution. The formation of a complex between ozone and bromide ion, $[O_3\cdots Br^-]$, which can lead to production of Br_2 by reaction at the air−water interface, is therefore feasible. Experimentally observed Br_2 is well predicted by including an interface process with a reaction probability of $[1.9 \pm 0.8] \times 10^{-6}$ (1 s) as the first step in a surface mechanism to produce additional gas-phase Br_2. An estimate of the impact of this interface reaction on bromine formation in the marine boundary layer shows that several ppt of bromine could potentially be produced during the night from this proposed surface chemistry.

1. Introduction

A number of field studies in both the Arctic and mid-latitude regions have verified the presence of inorganic bromine in the marine boundary layer.[1−7] The importance of bromine in the chemistry of the troposphere arises primarily from its influence on ozone. Recent evidence suggests that bromine also plays a role in determining gas-phase mercury concentrations.[8−16] Barrie and co-workers first recognized the relationship of bromine with ozone when they observed an increase in the amount of filterable bromine collected during periods of ozone depletion in the Arctic.[2] A number of field studies subsequently confirmed that gas-phase halogens were formed in the Arctic marine boundary layer.[3−7] Notably, increased concentrations of molecular bromine and bromine chloride were measured during episodes of surface level ozone depletion in the Arctic after polar sunrise.[5−7] Field studies show that increased concentrations of bromine species correlate to tropospheric ozone depletion in a variety of mid-latitude regions outside the Arctic as well.[17−22] The mechanism of ozone destruction begins with photolysis of the molecular bromine species to yield bromine atoms, which destroy ozone in a well-known cycle involving BrO_x and HO_x.[23]

The most likely source of bromine is sea salt particles, seawater ice, and frost flowers.[1,24−32] The impact of sea salt on tropospheric chemistry is well recognized and, although bromide ions are a minor component of sea salt, their role is disproportionately large. While bromide ions may be oxidized by a variety of atmospheric oxidants, including HSO_5^-,[33] N_2O_5,[24,34] NO_3,[35,36] OH,[37] and O_3,[38−41] ozone is likely to be an important oxidant, especially during the nighttime in unpolluted marine regions.

The chemistry of bromide ion oxidation by ozone in the aqueous phase has been studied in some detail.[42−48] It is known that bromide ions are oxidized by ozone to form hypobromous acid, HOBr, which then reacts with HBr to yield molecular bromine (R1, R2). This dissolved bromine is then readily transported into the gas phase.

$$O_3 + Br^- + H_2O \rightarrow HOBr + O_2 + OH^- \qquad (R1)$$

$$HOBr + Br^- + H^+ \rightarrow Br_2 + H_2O \qquad (R2)$$

However, the mechanism for gas-phase bromine formation from the reaction of O_3 with aqueous NaBr particles is still not well understood. Hirokawa and co-workers[39] studied the reaction of ozone with NaBr particles located on a glass fiber filter and reported that Br_2 was only observed in the presence of added water vapor. The generation of Br_2 from the reaction of ozone with deliquesced NaBr particles was also reported by De Haan et al.,[40] but neither case treated the kinetics. In their investigation of aqueous sodium bromide aerosol oxidation by ozone, Anastasio and Mozurkewich[41] observed a bromine production larger than anticipated from known aqueous phase chemistry; they proposed that the additional bromine was produced from bromide deposited on the surface of the glass reaction vessel.

The goal of the present work is to investigate the reaction of deliquesced NaBr particles with gas-phase O_3 using a combination of aerosol chamber experiments, chemical kinetics modeling, and molecular dynamics simulations. We show that the majority of the observed Br_2 production is due to the reaction of O_3 with bromide ions at the air−water interface rather than reactions in the bulk aqueous solution. This oxidation of bromide

* To whom correspondence should be addressed. BJFP: phone (949) 824-7670, fax (949) 824-3168; e-mail bjfinlay@uci.edu. DJT: phone (949) 824-4295, fax (949) 824-8571, e-mail dtobias@uci.edu.

† Current address: Institute of Organic Chemistry and Biochemistry and Center for Complex Molecular Systems and Biomolecules, Academy of Sciences of the Czech Republic, Flemingovo n. 2, 166 10 Prague 6, Czech Republic

‡ Current address: EPRI, 3412 Hillview Ave, Palo Alto, CA 94304.

§ Department of Mechanical & Aerospace Engineering.

10.1021/jp0467346 CCC: $27.50
Published on Web 11/26/2004

by O_3 at the interface may potentially produce several ppt of bromine in the marine boundary layer at night.

2. Methodology

2.1. Aerosol Chamber Experiments. Experiments were carried out in an aerosol chamber described in detail elsewhere.[40] Briefly, the system consists of a 561 L aluminum and stainless steel chamber equipped with White cell optics aligned for a path length of 52.5 m for the Fourier transform infrared spectroscopy (FTIR: Mattson, Infinity 60). Species in the chamber are also monitored with an atmospheric pressure ionization mass spectrometer (API-MS: Perkin-Elmer Sciex, Model API-300). In this tandem mass spectrometer, ions selected in the first quadrupole are collisionally dissociated to produce fragments selected in the second quadrupole. For this work, the Br_2 concentration was measured with mass ratio monitoring (MRM) in the negative ion mode using the ion pair with mass to charge ratios 158 and 79. Using the MRM mode ensures that all fragments of m/z 79 (^{79}Br) resulted only from parent ions of 158 ($^{79}Br_2$) rather than other bromine-containing species. Metal surfaces in the chamber were coated with Krytox LVP high-vacuum grease (Dupont) to minimize the reactivity of the surfaces. In addition, several initial experiments were performed with halocarbon wax (Halocarbon Products Inc., Series 1500) as a coating.

Two methods were used to produce NaBr particles of different size distributions. Smaller particles were generated by flowing ultrahigh purity nitrogen (Oxygen Services Co., 99.999%) through an atomizer (TSI Inc., Model 3076) that contained a 1% NaBr (Alfa Products, ultrapure) solution in Nanopure water (Barnstead, 18 MΩ·cm). The size distribution and concentration of these particles was measured with a scanning mobility particle sizer (SMPS: TSI Inc., Model 3071) and a condensation particle counter (CPC: TSI Inc., Model 3025A). Larger particles were produced by flowing nitrogen with a backing pressure of 20 psig through a 6-jet Collison nebulizer (BGI Inc., Model CN25) containing a saturated NaBr solution. The size distribution of the large particles was measured with an aerodynamic particle sizer (APS: TSI Inc., Model 3320). When sampling from the aerosol chamber, the median diameter of small particles produced with the atomizer was 170−250 nm and larger particles from the nebulizer had a median diameter of 750−850 nm. As discussed below, the concentration of the NaBr in the aqueous aerosol particles is dependent on the relative humidity (RH) and in these experiments it ranged from 4.3 M (∼85% RH) to 6.6 M (∼63% RH).

Aerosol particles were introduced into the chamber after it was filled with 680−730 Torr of ultrapure air (Scott-Marrin, total HC + CO < 0.01 ppm, NO_x < 0.001 ppm, SO_2 < 0.001 ppm) at a relative humidity above the deliquescence point of NaBr (58%). This ensured that the aerosol particles existed as concentrated aqueous salt solutions throughout the experiment. Mixtures of ozone in oxygen were generated by passing O_2 (Oxygen Services Co., 99.993%) through a commercial ozonizer (Polymetrics, Model T-816). After 5 to 10 min to allow mixing of the aerosol in the chamber, 0.35 to 1.6 ppm of ozone was introduced through a glass mixing tube. This tube, which is approximately 2 m long with small holes periodically spaced along the length, was positioned along the center of the chamber to decrease the mixing time of the reactant gas. Practical experimental considerations limited the range of ozone concentrations used in these experiments. At ozone concentrations greater than 1.6 ppm, the sensitivity of the API-MS to Br_2 decreased significantly, thus making accurate quantitation of the Br_2 concentration throughout the experiment difficult. The minimum ozone concentration was chosen to be low enough to approach atmospheric conditions, but also high enough to yield a measurable Br_2 production during a reasonable experimental time.

In each experiment, the reaction was continuously monitored with FTIR and API-MS for 60 min, with sampling of the aerosol particle size distribution at the beginning and end of this period. For about 5 min at the beginning and end of each experiment, a sample from the chamber was passed through an annular glass denuder coated with potassium carbonate (K_2CO_3: EM Science, ≥99.0%) and glycerol (EM Science, 99.5%) to remove gaseous halogen species. The signals measured while passing the sample through the denuder represent the background, which includes any Br_2 that might be formed from particles in the corona discharge region of the API-MS. In a typical experiment, the background Br_2 signal was approximately 5−10% of the peak Br_2 formed. Calibrations were performed at the end of each experiment by adding to the aerosol chamber a known amount of gaseous Br_2 obtained from the vapor over the liquid (Fluka, ≥99.5% purity). A number of experiments were performed while varying parameters such as the total amount of aerosol, the initial ozone concentration, the relative humidity, and the aerosol size.

Since aerosol particles and gas-phase bromine species adsorb onto the walls of the chamber, it was cleaned between experiments to decrease the effects of contamination. Cleaning was performed by rinsing the chamber with Nanopure water. Blank experiments with no aerosol present were performed after cleaning as well as between aerosol experiments to ensure that the effects of wall contamination were small.

While the Krytox wall coating minimized reaction and loss processes occurring on the chamber walls, the loss of Br_2 was still significant relative to the amount produced from the reaction with ozone. The rate of Br_2 wall loss varied in each experiment since it is dependent on the amount of wall contamination from previous experiments as well as on experimental conditions such as relative humidity. Therefore, for each experiment on the reaction of ozone with NaBr aerosol, a corresponding experiment was performed to determine the wall loss under similar experimental conditions. In these wall loss experiments, approximately 15 ppb Br_2 was added to the chamber along with similar amounts of aerosol. The bromine concentration in the aerosol chamber was then monitored for 60 min and aerosol measurements were taken as before. Wall loss experiments performed before and after O_3 + NaBr experiments showed that the loss rate does not change significantly during the course of a single experiment.

Both the API-MS and the aerosol measurement systems require sampling contents from the chamber. To maintain a constant pressure in the system, a collapsible Teflon reaction chamber, filled with humid air at the same RH as the aerosol chamber, was connected to the chamber. When sampling with the API-MS or the aerosol measurement systems, air from the collapsible Teflon chamber flowed into the aerosol reaction chamber and diluted the reaction mixture. Flow rates into the instruments were measured to incorporate this dilution into the kinetics model as discussed below.

2.2. Chemical Kinetics Model. A computational chemical kinetics box model was used to explore the mechanism of Br_2 production in this system. The model, MAGIC (Model of Aqueous, Gas, and Interface Chemistry), was developed previously for use with NaCl experiments and has been described in detail elsewhere.[49] MAGIC includes chemical reactions and

TABLE 1: Species Included in the Kinetics Model[a]

group	gas phase	aqueous phase
HO_x	$O(^1D)$, $O(^3P)$, **O_2**, **O_3**, **OH**, **HO_2**, **H_2O_2**, H_2O	$O(^3P)$, **O_2**, **O_3**, **OH**/O^-, **HO_2**/O_2^-, **H_2O_2**/HO_2^-, HO_3, O_3^-, H^+/OH^-
BrO_x	Br, **Br_2**, **HBr**, BrO, **HOBr**	Br, **Br_2**, **HBr**/Br^-, Br_2^-, Br_2O_4, Br_3^-, BrO, **HOBr**/BrO^-, BrO_2, $HBrO_2$/BrO_2^-, BrO_3^-, $HOBr^-$
CO_2	**CO_2**	**CO_2·H_2O**/HCO_3^-/CO_3^{2-}, HCO_3/CO_3^-
other	N_2	Na^+

[a] Species in bold are transferred between the gas and the aqueous phase.

diffusion in both the gas and aqueous phase, and mass transfer between the phases, which is treated according to the method defined by Schwartz.[50] This model assumes that electrolytic species and their dissociated products react while preserving neutrality and equilibrium.

For this work, the previous version of MAGIC has been expanded to include bromine chemistry with an additional 13 gas phase and 69 aqueous phase reactions. Species included in MAGIC are listed in Table 1 and the additional reactions are presented in Tables 2 and 3. Data for the additional bromine species that undergo mass transfer between the two phases (Br_2, HBr, and HOBr) are listed in Table 4 and equilibrium expressions for bromine species are shown in Table 5. Finally, reactions, rate constants, and physical constants for the HO_x species are discussed in ref 49. Changes implemented in MAGIC are discussed subsequently.

Margerum and co-workers have shown that the hydrolysis of Br_2 occurs via a general acid/base assisted mechanism in aqueous solution.[54] Consequently, reactions of the overall form

$$Br_2 + H_2O + A^- \leftrightarrow HOBr + Br^- + HA \qquad (R3)$$

involve a transition state such as

$$A^- \cdots H - \overset{H}{\overset{|}{O}} \cdots Br - Br \leftrightarrow A - H \cdots \overset{H}{\overset{|}{O}} - Br \cdots Br^- \qquad (R4)$$

and the rate constants are proportional to the strength of the assisting acid or base according to the Brønsted−Pederson equations[80]

$$\log\left(\frac{k_{\rightarrow}}{q}\right) = \log G_B - \beta \log\left(\frac{K_a q}{p}\right) \qquad (E1)$$

$$\log\left(\frac{k_{\leftarrow}}{p}\right) = \log G_A - \alpha \log\left(\frac{K_a q}{p}\right) \qquad (E2)$$

where $k_{\rightarrow}$ and $k_{\leftarrow}$ are the forward and reverse rates of reaction R3, q is the number of sites on the conjugate base (A^-) that can accept a proton, and p is the number of equivalent protons on the acid (HA). The constants α and β theoretically add up to unity and reflect the degree of proton transfer in the transition state; G_A and G_B are proportionality constants. As discussed previously,[49] the use of the H_3O^+/H_2O acid−base pair in the Brønsted−Pederson relationship is often not valid because these species are of a different type and charge than the other acid−base pairs. Consequently, the rate constants for reactions A10−A15 and A18−A19 were derived from the Brønsted−Pederson relationship according to eqs E1 and E2 by using the rate constants developed by Beckwith et al.,[54] but excluding the point for the acid H_3O^+. The resulting values are 0.49 and 0.51 for α and β, respectively, rather than 0.22 and 0.78 as determined by Beckwith et al. with the inclusion of H_3O^+ data. Similarly, the resulting proportionality constants used in these calculations were $G_A = 10^{9.89}$ and $G_B = 10^{1.68}$.

The original version of MAGIC used to study NaCl reactions included hypochlorite (ClO^-) as the most oxidized form of the halogen in solution.[49] However, since the oxidation of bromine species typically occurs at least an order of magnitude faster than for chlorine species, both bromite (BrO_2^-) and bromate (BrO_3^-) are expected to form and are included in the current version of MAGIC, as shown in Tables 1 and 3.

Several of the reactions involve radical species that are produced in the aqueous phase from the slow reaction[81] of ozone with hydroxide ion.

$$O_3 + OH^- \rightarrow HO_2 + O_2^- \qquad (R5)$$

While the resulting concentrations of radical species are certainly small in the absence of photochemistry, this version of MAGIC was developed for analysis of experiments that also involved the reaction with hydroxyl radical. In the interest of completeness, the entire reaction mechanism is included.

The initial NaBr molality of the droplets was calculated from the measured relative humidity based on the relationship between water activity and molality.[82] Molarity was calculated from molality based on published density data for NaBr solutions[83] and additional experiments performed in this laboratory over a wider range of NaBr concentrations.

The rate of dilution of the chamber due to sampling into the API-MS and aerosol measurement systems was incorporated

TABLE 2: Gas-Phase Bromine Chemistry[a]

no.	reaction	A	E/R	k_{298}	ref
G1	$O + BrO \rightarrow Br + O_2$	1.9×10^{-11}	−230	4.11×10^{-11}	51, 52
G2	$O + HBr \rightarrow OH + Br$	5.8×10^{-12}	1500	3.78×10^{-14}	51
G3	$O + HOBr \rightarrow OH + BrO$	1.2×10^{-10}	430	2.83×10^{-11}	51, 52
G4	$OH + Br_2 \rightarrow HOBr + Br$	4.2×10^{-11}	0	4.25×10^{-11}	52
G5	$OH + BrO \rightarrow Br + HO_2$			7.50×10^{-11}	51, 52
G6	$OH + HBr \rightarrow H_2O + Br$	1.1×10^{-11}	0	1.10×10^{-11}	51, 52
G7	$HO_2 + Br \rightarrow HBr + O_2$	1.4×10^{-11}	590	1.93×10^{-12}	52
G8	$HO_2 + BrO \rightarrow HOBr + O_2$	3.7×10^{-12}	−545	2.30×10^{-11}	52
G9	$Br + O_3 \rightarrow BrO + O_2$	1.7×10^{-11}	800	1.16×10^{-12}	51, 52
G10	$Br + H_2O_2 \rightarrow HBr + HO_2$			5.00×10^{-16}	51, 52
G11	$BrO + O_3 \rightarrow Br + O_2 + O_2$			2.00×10^{-17}	51, 52
G12	$BrO + BrO \rightarrow Br + Br + O_2$	2.70×10^{-12}		2.70×10^{-12}	52
G13	$BrO + BrO \rightarrow Br_2 + O_2$	2.90×10^{-14}	−840	4.86×10^{-13}	52

[a] Rate constants for bimolecular reactions are given by $k = A \exp(-E/RT)$ in units of $cm^3molecule^{-1}s^{-1}$, A is the Arrhenius factor in $cm^3molecule^{-1}s^{-1}$, and E is the activation energy.

TABLE 3: Aqueous Phase Bromine Chemistry[a]

no.	reaction	K_{298}	ref	no.	reaction	K_{298}	ref
A1	$Br^- + O_3 + H_2O \rightarrow HOBr + O_2 + OH^-$	258	42	A35	$HOBr^- \rightarrow Br + OH^-$	4.20×10^6	63
A2	$BrO^- + O_3 \rightarrow Br^- + O_2 + O_2$	330	43	A36	$Br + OH^- \rightarrow HOBr^-$	1.30×10^{10}	64
A3	$BrO^- + O_3 \rightarrow BrO_2^- + O_2$	100	43	A37	$HOBr^- + H^+ \rightarrow Br + H_2O$	4.40×10^{10}	63
A4	$HOBr + O_3 \rightarrow BrO_2^- + O_2 + H^+$	0.013	43	A38	$Br + H_2O \rightarrow HOBr^- + H^+$	1.36	65
A5	$BrO_2^- + O_3 \rightarrow BrO_3^- + O_2$	1.00×10^5	43	A39	$HOBr^- + Br^- + \rightarrow Br_2^- + OH^-$	1.90×10^8	63
A6	$Br_2 + Br^- \rightarrow Br_3^-$	1.50×10^9	53	A40	$Br_2^- + OH^- + \rightarrow HOBr^- + Br^-$	2.70×10^6	*d*
A7	$Br_3^- \rightarrow Br_2 + Br^-$	5.00×10^7	53	A41	$Br + Br^- + \rightarrow Br_2^-$	1.20×10^{10}	66
A8	$Br_2 + H_2O \rightarrow HOBr + Br^- + H^+$	97	54	A42	$Br_2^- \rightarrow Br + Br^-$	1.90×10^4	66
A9	$HOBr + Br^- + H^+ \rightarrow Br_2 + H_2O$	1.60×10^{10}	54	A43	$Br_2^- + Br_2^- \rightarrow Br_3^- + Br^-$	2.40×10^9	67
A10	$HOBr + Br^- + H_2O \rightarrow Br_2 + OH^- + H_2O$	3.20×10^4	54[b]	A44	$Br + Br \rightarrow Br_2$	5.00×10^9	66
A11	$Br_2 + OH^- + H_2O \rightarrow HOBr + Br^- + H_2O$	7.00×10^9	54[b]	A45	$Br + Br_2^- \rightarrow Br_2 + Br^-$	5.00×10^9	66
A12	$Br_2 + HCO_3^- + H_2O \rightarrow HOBr + Br^- + CO_2H_2O$	1.60×10^5	54[b]	A46	$Br + BrO^- \rightarrow Br^- + BrO$	4.10×10^9	65
A13	$HOBr + Br^- + CO_2H_2O \rightarrow Br_2 + HCO_3^- + H_2O$	1.20×10^7	54[b]	A47	$Br_2^- + BrO^- \rightarrow BrO + Br^- + Br^-$	8.00×10^7	45
A14	$Br_2 + CO_3^{2-} + H_2O \rightarrow HOBr + Br^- + HCO_3^-$	1.50×10^7	54[b]	A48	$Br_2^- + BrO_2^- \rightarrow BrO + BrO^- + Br^-$	8.00×10^7	45
A15	$HOBr + Br^- + HCO_3^- \rightarrow Br_2 + CO_3^{2-} + H_2O$	1.10×10^5	54[b]	A49	$BrO + BrO + H_2O \rightarrow BrO^- + BrO_2^- + H^+ + H^+$	2.80×10^9	65
A16	$BrO^- + HCO_3^- \rightarrow HOBr + CO_3^{2-}$	3.90×10^7	55	A50	$BrO_2 + BrO_2 \rightarrow Br_2O_4$	6.00×10^9	68
A17	$HOBr + CO_3^{2-} \rightarrow BrO^- + HCO_3^-$	3.00×10^8	55	A51	$Br_2O_4 \rightarrow BrO_2 + BrO_2$	3.10×10^5	68
A18	$Br_2 + HO_2^- + H_2O \rightarrow HOBr + Br^- + H_2O_2$	8.80×10^7	54[b]	A52	$BrO + BrO_2^- \rightarrow BrO^- + BrO_2$	3.40×10^8	45
A19	$HOBr + Br^- + H_2O_2 \rightarrow Br_2 + HO_2^- + H_2O$	3.90×10^4	54[b]	A53	$BrO^- + CO_3^- \rightarrow BrO + CO_3^{2-}$	4.30×10^7	45
A20	$HOBr + H_2O_2 \rightarrow Br^- + O_2 + H^+ + H_2O$	1.50×10^4	56	A54	$BrO_2^- + CO_3^- \rightarrow BrO_2 + CO_3^{2-}$	5.00×10^7	69
A21	$HOBr + HO_2^- \rightarrow Br^- + O_2 + H^+ + H_2O$	7.60×10^8	57	A55	$Br + H_2O_2 \rightarrow Br^- + HO_2 + H^+$	2.50×10^9	70
A22	$Br^- + H_2O_2 + H^+ \rightarrow HOBr + H_2O$	1.40×10^{-2}	58	A56	$Br_2^- + H_2O_2 \rightarrow Br^- + Br^- + HO_2 + H^+$	1.00×10^3	70
A23	$Br^- + H_2O_2 \rightarrow HOBr + OH^-$	2.30×10^{-5}	58	A57	$Br_2 + HO_2 \rightarrow Br_2^- + O_2 + H^+$	1.30×10^8	71
A24	$BrO^- + BrO^- \rightarrow BrO_2^- + Br^-$	6.00×10^{-7}	59	A58	$Br_2^- + HO_2 \rightarrow Br_2 + HO_2^-$	3.80×10^9	70
A25	$HBrO_2 + BrO_2^- \rightarrow HOBr + BrO_3^-$	39.1	60	A59	$Br_3^- + HO_2 \rightarrow Br_2^- + Br^- + O_2 + H^+$	1.00×10^7	44
A26	$HOBr + HOBr + CO_3^{2-} \rightarrow HBrO_2 + Br^- + HCO_3^-$	0.32	59	A60	$Br_2 + O_2^- \rightarrow Br_2^- + O_2$	5.00×10^9	71
A27	$HOBr + HOBr + OH^- \rightarrow HBrO_2 + Br^- + H_2O$	15	59	A61	$Br_3^- + O_2^- \rightarrow Br_2^- + Br^- + O_2$	1.50×10^9	71
A28	$HOBr + HOBr \rightarrow HBrO_2 + Br^- + H^+$	2.00×10^{-3}	59	A62	$BrO^- + O_2^- + H_2O \rightarrow Br + O_2 + OH^- + OH^-$	2.00×10^8	71
A29	$HBrO_2 + HBrO_2 \rightarrow HOBr + BrO_3^- + H^+$	800	60	A63	$HOBr + O_2^- \rightarrow Br + O_2 + OH^-$	3.50×10^9	71
A30	$Br_2O_4 + OH^- \rightarrow BrO_3^- + BrO_2^- + H^+$	7.00×10^8	45	A64	$HOBr + OH \rightarrow BrO + H_2O$	2.00×10^9	65
A31	$BrO_2^- + O(^3P) \rightarrow BrO^- + O_2$	1.24×10^9	61[c]	A65	$BrO^- + OH \rightarrow BrO + OH^-$	4.50×10^9	45
A32	$BrO_3^- + O(^3P) \rightarrow BrO_2^- + O_2$	1.50×10^7	62	A66	$BrO_2 + OH \rightarrow BrO_3^- + H^+$	2.00×10^9	68
A33	$Br^- + OH \rightarrow HOBr^-$	1.06×10^{10}	63	A67	$BrO_2^- + OH \rightarrow BrO_2 + OH^-$	1.90×10^9	45
A34	$HOBr^- \rightarrow Br^- + OH$	3.30×10^7	63	A68	$BrO^- + O^- + H_2O \rightarrow BrO + OH^- + OH^-$	4.60×10^9	45
				A69	$BrO_2^- + O^- + H_2O \rightarrow BrO_2 + OH^- + OH^-$	1.10×10^9	72

[a] Rate constants for unimolecular, bimolecular, and termolecular reactions in units of s^{-1}, $M^{-1}\ s^{-1}$, and $M^{-2}\ s^{-1}$, respectively. Water is not included in any of the rate expressions. [b] Calculated by using the Alternate Brønsted Extrapolation. See text for details. [c] $k = 0.31k[O(^3P) + O_2]$, where $k[O(^3P) + O_2] = 4.0 \times 10^9$ as in ref 62. [d] Using k of reaction A39 from ref 63 and K from ref 37.

TABLE 4: Physical Solubility Constants and Accommodation Coefficients for Bromine Species

species	H_{298} (M atm^{-1})	ref	α	ref
Br_2	0.77	73	0.038	74
HBr	0.706[a]	75, 76	0.018	77
HOBr	1.85×10^3	78	0.6	79

[a] Reported value is H/K_a. Use K_a given in Table 5 to obtain H_{298}.

TABLE 5: Aqueous Phase Equilibrium Constants of Bromine Species

species	$K_{a,298}$ (M)	ref
$HBr \leftrightarrow H^+ + Br^-$	1.00×10^9	77
$HOBr \leftrightarrow H^+ + BrO^-$	1.58×10^{-9}	55
$HBrO_2 \leftrightarrow H^+ + BrO_2^-$	3.72×10^{-4}	60

into MAGIC as a first-order loss process as discussed previously.[49] The dilution factor used was calculated from the chamber volume and the measured flow rate into each instrument.

2.3. Molecular Dynamics Simulations. To investigate the interaction of ozone with the aqueous NaBr particles at a molecular level, classical molecular dynamics (MD) simulations were performed with the AMBER 6 program package.[84] The simulations were carried out for 1.2 and 6.1 M NaBr concentrations. The higher concentration corresponds to that of typical experimental conditions in the aerosol chamber, while comparison with the dilute system gives insight into the effects of varying concentration. In the 1.2 M case, the system consisted of 864 water molecules, 18 Na^+ ions, and 18 Br^- ions; while in the 6.1 M case, it was comprised of 864 water molecules, 96 Na^+ ions, and 96 Br^- ions, both in a $30(x) \times 30(y) \times 100(z)$ Å^3 simulation box. Applying periodic boundary conditions in all three dimensions yielded infinite slabs, each possessing two vacuum/liquid interfaces, with the z axis normal to the interface. The thicknesses of the 1.2 and 6.1 M solution slabs were roughly 40 and 45 Å, respectively. The location of the interface is slightly different for the 1.2 M solution compared to that of the 6.1 M one, as the latter system contains a larger number of ions in an identical simulation box, resulting in an increased thickness of the slab. Both solutions were equilibrated for 0.5 ns at 300 K prior to the addition of ozone molecules.

To study ozone interactions with the NaBr solution, five O_3 molecules were added into the simulation box approximately 10 Å above the solution surface, at random positions in the xy plane, and were assigned a small initial velocity (0.1 m s^{-1}) toward the slab. In addition, a simulation initiated with all five O_3 molecules fully solvated inside the 1.2 M solution was carried out. To prepare the initial configuration for this simulation, five randomly selected water molecules located inside the bulk liquid (at a z-position -5 Å $\leq z \leq 5$ Å) were replaced by ozone molecules and moved into the gas phase above the liquid slab. A 20-ps equilibration run with an integration time step of 0.1 fs was performed, at the end of which the five water molecules were back in the liquid phase, and all five O_3 molecules

TABLE 6: Force Field Parameters for Molecular Dynamics Simulations

species	q (e)	α (Å^3)	r_m (Å)	ϵ (kcal/mol)
Na^+	1.0	0.24	1.532	0.100
Br^-	−1.0	4.53	2.577	0.170
H_2O[a]				
O	−0.730	0.528	1.798	0.156
H	0.365	0.170	0	0
O_3[b]				
O_{center}	0.190	0.95	1.798	0.156
O_{side}	−0.095	0.95	1.798	0.156

[a] r(O−H) = 1.0 Å, β(H−O−H) = 109.5°. [b] r(O−O) = 1.28 Å, $\beta(O_{side}-O_{center}-O_{side})$ =116.7°.

remained fully solvated inside the bulk solution, close to the middle of the slab.

The systems were propagated for 1 ns with a time step of 1 fs. A constant temperature of 300 K was maintained throughout the simulation by using the Berendsen scheme with a coupling constant of 0.5.[85] All bond lengths were constrained to their equilibrium values with SHAKE.[86] An interaction cutoff of 12 Å was employed, and the smooth particle mesh Ewald method was used to account for the long-range Coulomb interactions.[87] The positions of all atoms were stored every picosecond.

Empirical potentials that explicitly include induced polarization were employed. The force field parameters are summarized in Table 6. The potentials for ions were adopted from Jungwirth and Tobias,[88] and water molecules were described by using the POL3 model.[89] The Lennard-Jones parameters of the O_3 oxygen atoms were also taken from the POL3 water model. The geometric parameters of the ozone molecule, r(O−O) = 1.284 Å and $\beta(O_{side}-O_{center}-O_{side})$ = 116.7°, were calculated by the ab initio MP2/aug-cc-pvtz optimization performed by using the GAUSSIAN 98 program package.[90] The partial charges of −0.095e on the side oxygens and +0.19e on the central oxygen were chosen to match the experimental value of the permanent dipole moment of ozone molecule (0.53 D)[91] for the above geometry. The molecular polarizability of ozone, α_m = 2.85 Å^3, was obtained as the mean value of the diagonal elements of the polarizability tensor calculated at the CCSD(T)/7s5p4d2f level by Maroulis.[91] One-third of this value, $\alpha_m/3$ = 0.95 Å^3, was then assigned to each of the three oxygen atoms of the ozone molecule. The present ozone force field represents a refinement of the one employed in the previous study[92] in terms of the electric properties of the ozone molecule and their agreement with experiment.[91] The increased magnitude of the permanent dipole moment μ and molecular polarizability α_m of ozone in the present parametrization (μ = 0.53 D and α_m = 2.85 Å^3, as opposed to μ = 0.34 D and α_m = 2.31 Å^3 used previously[92]) results in roughly 30% greater O_3−water binding energy and, consequently, in a stronger interaction of ozone with the NaBr solution slab.

The new O_3 parametrization was tested against ab initio results for $[O_3\cdots H_2O]$ and $[O_3\cdots Br^-]$ complexes. For the $[O_3\cdots H_2O]$ complex, it yielded a binding energy of 1.3 kcal mol^{-1}, which is in good agreement with an ab initio calculated $[O_3\cdot H_2O]$ binding energy of 1.6 kcal mol^{-1},[93] and falls within the range of ab initio values, 0.7−2.4 kcal/mol, reported in the literature.[94,95] The $[O_3\cdot Br^-]$ binding energy was underestimated by about 1 kcal/mol compared to the ab initio value of 5.8 kcal/mol.[96] In terms of ozone solvation in liquid water, the present force field results in the solvation of ozone in bulk water being less favorable in the simulation compared to experimental conditions, as it overestimates the standard hydration free energy of ozone by 0.8 kcal/mol[97] compared to the experimental value of ΔG° = 2.73 kcal/mol (corresponding to the Henry's law constant k_H = 0.01 M/atm[98]).

3. Results and Discussion

3.1. Chamber Experiment and Kinetics Modeling. Twelve experiments were carried out in which the production of gas-phase Br_2 from the reaction of O_3 with deliquesced NaBr particles was measured. Table 7 summarizes the conditions in five experiments which are representative of the results observed in a larger number of experiments in which the amount and average size of the aerosol, the relative humidity, and the ozone concentration were systematically varied.[99] Figure 1 shows the ozone loss and bromine production in the representative experiments for which the reaction conditions are detailed in Table 7. During the first 10−15 min after the addition of ozone to the chamber, the chamber contents became thoroughly mixed and the total pressure equalized between the chamber and the Teflon ballast; because these factors impacted the API-MS sensitivity, these initial data were less precise and hence were not used in the model analysis. The solid lines in the figure represent the model predicted values, which include dilution during sampling from the chamber as well as known gas phase and bulk aqueous phase chemistry. The ozone data are reason-

TABLE 7: Experimental and Model Parameters for Representative Experiments

parameter	units	base case	less aerosol	high RH	less O_3	larger aerosol
aerosol:[a]						
number concentration[b]	number cm^{-3}	2.92×10^5	1.65×10^5	2.47×10^5	2.40×10^5	1.97×10^4
volume	cm^3/m^3	3.53×10^{-3}	1.03×10^{-3}	3.87×10^{-3}	3.92×10^{-3}	6.15×10^{-3}
surface area	cm^2/cm^3	4.68×10^{-4}	1.57×10^{-4}	4.45×10^{-4}	4.53×10^{-4}	3.95×10^{-4}
median diameter	nm	285	228	311	306	842
mass transfer radius	nm	224	198	258	256	466
surface/volume	cm^{-1}	1.3×10^5	1.5×10^5	1.2×10^5	1.2×10^5	6.4×10^4
relative humidity	%	67	71	85	64	66
$[O_3]_0$	ppm	1.55	1.54	1.54	0.35	1.61
$[CO_2]_0$	ppm	3.0	1.2	11.0	10.0	2.7
$[NaBr]_0$	M	5.9	5.6	4.4	6.5	6.1
$k(Br_2)_{wall\ loss}$	s^{-1}	8.0×10^{-5}	9.0×10^{-5}	9.0×10^{-5}	6.0×10^{-5}	8.0×10^{-5}
$k(CO_2)_{gen}$ (see ref 99)	molec cm^{-3} s^{-1}	3.0×10^{10}	1.5×10^{11}	1.5×10^{11}	7.0×10^{10}	4.0×10^{10}
after 60 min reaction:						
$[Br_2]_{exp}$	ppb	20.5	5.5	13.6	5.1	19.0
$[Br_2]_{known\ chemistry}$	ppb	1.48	0.41	1.46	0.37	2.66
$\gamma_{surface\ rxn}$		2.8×10^{-6}	1.6×10^{-6}	1.6×10^{-6}	1.5×10^{-6}	2.4×10^{-6}

[a] Aerosol data are an average of measurements taken at the beginning and end of each experiment. [b] Number concentration is the number of particles with the median diameter needed to reproduce the total aerosol volume. Data from aerosol measurements were fit to a log-normal distribution and integrated to include aerosol outside the size range of the instruments.

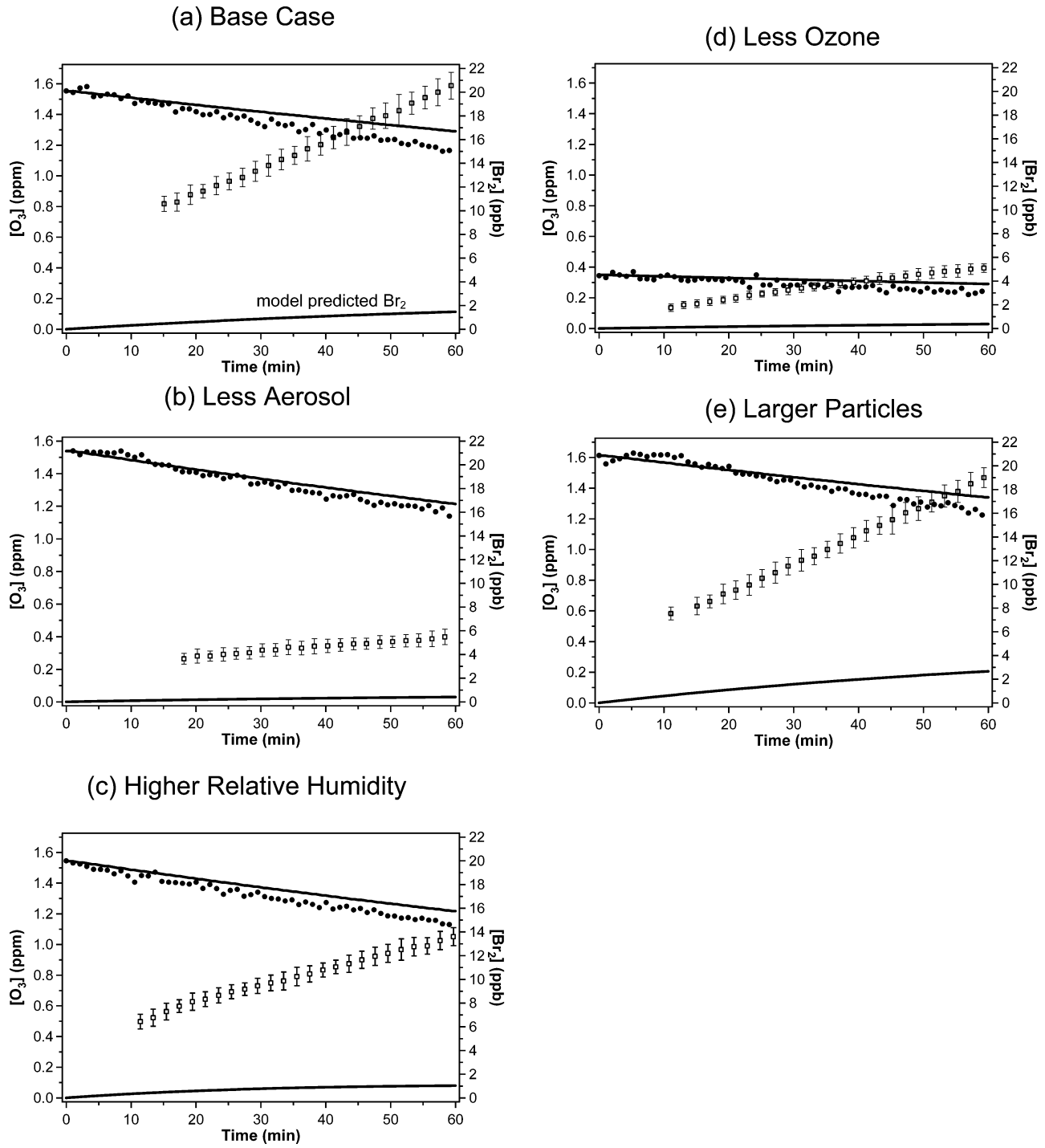

Figure 1. Reaction−time profiles of O_3 and Br_2 in five representative aerosol chamber experiments corresponding to (a) the base case experiment, (b) less aerosol, (c) higher relative humidity, (d) less ozone, and (e) larger particles. Filled circles and open squares denote experimental ozone and bromine concentrations, respectively. Solid lines indicate the concentrations predicted with MAGIC, using known gas and aqueous phase chemistry. A summary of the experimental conditions is given in Table 7.

ably well matched by the model, although there is a tendency for the O_3 to decay slightly faster than predicted. However, in all cases the bromine production is underpredicted by approximately a factor of 10. The dramatic underprediction is also seen by a comparison of the measured bromine concentrations after 60 min of reaction time to those predicted based on known gas and aqueous phase chemistry (Table 7).

Because of these unexpected, but quite large, differences between the predicted and measured Br_2 concentrations during the reaction of deliquesced NaBr particles with ozone, a number of potential sources of the discrepancy were probed in detail. The first issue is the acidification of the droplets by uptake of gas-phase CO_2 in the chamber. As noted previously, bromine formation in the aqueous phase is initiated by the reaction of ozone with bromide ions:

$$Br^- + O_3 + H_2O \rightarrow HOBr + O_2 + OH^- \qquad (R6)$$

Liu et al.[42] report that this reaction is assisted by a general acid, H^+. According to the kinetics model that includes known gas and aqueous phase chemistry of bromine species, HO_x, and CO_2, the pH of the NaBr droplets is approximately 6.6 throughout

the period of the dark reaction. Therefore, it is not likely that acidic conditions in the aerosol droplets are increasing the reaction rate. Although the CO_2 concentration rose by as much as 25 ppm during the course of an experiment, increasing the CO_2 concentrations in the kinetics model by an order of magnitude does not affect the predicted amount of bromine formation. Therefore, the additional Br_2, above that expected for bulk aqueous phase reactions inside the particles, does not result from increased acidity of the system due to uptake of CO_2.

A second potential source of this discrepancy is uncertainty in the particle size distributions and concentrations. The values used in the kinetics model are an average of measurements obtained at the beginning and end of the reaction. In the case of the experiments with smaller aerosol, the observed changes in the average aerosol size and concentration are in agreement with those predicted from coagulation rates.[100] For the larger aerosol, the deposition is an order of magnitude faster and the measured aerosol size is smaller by a few nanometers at the end of the experiment due to preferential loss of the larger particles. The errors in the measurement of the aerosol size and number concentration are ±5 nm and ±20%, respectively. However, both of these errors are smaller than the amount of change in the aerosol distribution throughout the experiment. For example, while the number concentration decreases by 25−40% for both aerosol sizes, the median diameter increases approximately 40 nm (~30%) for the smaller aerosol, but remains nearly constant for the larger aerosol. To test the effect of the uncertainty in the aerosol measurements, the base case experiment was modeled by using three sets of aerosol data: (1) measurements at the beginning of the experiments, (2) measurements at the end of the experiments, and (3) an average of these values. Varying the aerosol data among these values affected the Br_2 formation predicted by MAGIC by less than 0.5 ppb. Consequently, uncertainty in the aerosol measurements is not a significant contributor to the underprediction of bromine.

As mentioned in the previous section, the updated version of MAGIC includes higher oxidized forms of the halogen in solution (bromite and bromate) to better represent the conditions in the experimental chamber. Model simulations performed excluding the bromite/bromate chemistry show that the amount of Br_2 formed is unchanged. Thus, the effect of this chemistry does not account for the extra bromine observed.

To assess the discrepancy between the observed bromine production and that predicted by MAGIC, the rate of the aqueous phase reaction of bromide ion with ozone, A1, was varied from 258 M^{-1} s^{-1}, the literature value from Liu et al.[42] To reproduce the observed bromine production, the rate constant must be increased by an order of magnitude to values of $(2-9) \times 10^3$ M^{-1} s^{-1}. These values lie well outside of the uncertainty of the rate reported by Liu and co-workers.[42] Several previous investigations of this reaction also report rate constants for this reaction over the range of 27 to 301 M^{-1} s^{-1},[43,56,101−103] all of which are significantly smaller than those required to fit the data.

In short, MAGIC underpredicts the Br_2 concentrations by about an order of magnitude, which is well outside the uncertainties in the experimental parameters and the bulk aqueous phase chemistry. These results indicate that processes not simulated by the standard gas and aqueous phase mechanisms are major contributors to bromine production in these experiments.

In previous experiments on the reaction of deliquesced NaCl aerosols with gas-phase OH, excess Cl_2 was observed that was more than 3 orders of magnitude greater than expected from uptake of OH into the particles and reaction in the bulk liquid. However, a good match to the experimental data was obtained if a reaction at the air−water interface between chloride ions and hydroxyl radicals was included in the model.[104] Further investigations of NaCl particle composition support this proposed interface reaction[105] and several other examples of reactions at interfaces were reported both before and after the NaCl studies.[74,106−112] Such evidence clearly indicates that reactions occurring at the air−water interface of particles can be important.

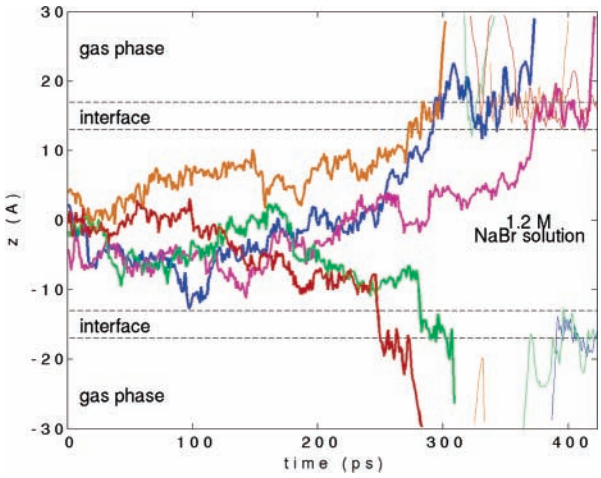

Figure 2. Trajectories of five O_3 molecules initially fully solvated inside the 1.2 M NaBr solution. The initial parts of the trajectories, until the first desorption of each ozone from the surface, are depicted by thick lines; thin lines are used to depict the subsequent collisions of the ozone molecules with the surface.

Consequently, the possibility that an interface reaction involving the formation of a complex between bromide ion and ozone may be occurring was considered. The plausibility of such interface reactions is supported by much theoretical work that shows that, contrary to classical theory of electrolyte solutions, halide ions are, in fact, present at the air−water interface of sodium halide solutions.[113,114]

3.2. Molecular Dynamics Results and Discussion. Previous work[92] on ozone interacting with water and aqueous salt solutions indicated a strong preference of the O_3 molecule for surface solvation rather than solvation in the bulk liquid. To examine the propensity of ozone for the air−liquid interface in the case of the NaBr solution, a 1-ns simulation was performed on five O_3 molecules initially fully solvated inside a 1.2 M solution. The ozone molecules were at first observed to diffuse throughout the interior of the liquid slab; however, within less than 400 ps all of them reached one of the two interfaces, and eventually desorbed. This part of the trajectories is shown in Figure 2, in which the *z*-position of the central oxygen atom of the five O_3 molecules is depicted as a function of time. The two air/liquid interfaces, defined by the regions between 10% and 90% of the liquid water density, are indicated by the dashed horizontal lines. Due to the periodic boundary conditions, whenever an ozone molecule desorbs from the surface and leaves the simulation box, its replica enters the box from the opposite side with the same velocity. Thus, a constant number of particles is maintained during the simulation and multiple collisions of ozone with the liquid surface can be observed. During the rest of the simulation, none of the ozone molecules entered the bulk liquid again, except occasionally for a few picoseconds, after which they returned back to the surface.

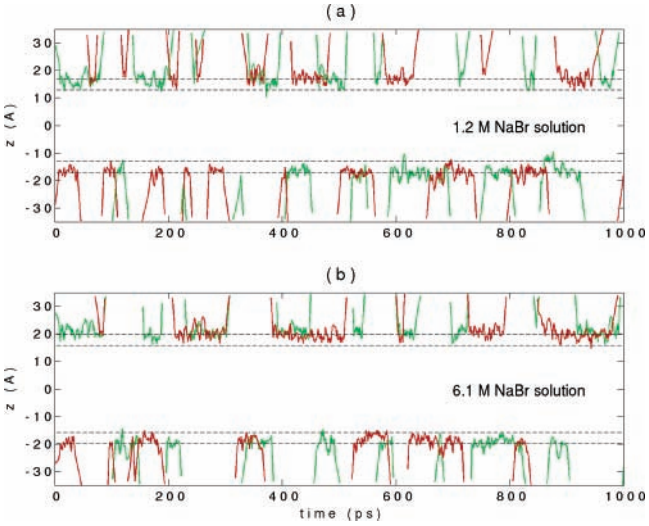

Figure 3. Representative trajectories of two ozone molecules (one depicted in red, the other in green) interacting with (a) 1.2 and (b) 6.1 M NaBr solution. The two air−liquid interfaces of the NaBr solution slabs, defined in each case by the regions between 10% and 90% of the liquid water density, are indicated by the dashed horizontal lines.

To further explore the interaction of ozone with the aqueous NaBr solution, 1-ns trajectories of five ozone molecules initiated from a position above the surface of the liquid solution equilibrated at 300 K were generated. Simulations were performed for 1.2 and 6.1 M solutions. Representative ozone trajectories are shown in Figure 3. For both NaBr concentrations, the ozone molecules are predominantly located in either of the two interfacial regions, entering the bulk solution only rarely and for very short periods of time. For the purpose of calculating the residence times of O_3 on the surface of the NaBr solution slab, a modified definition of the interfacial region is more appropriate than the standard definition based on 90% and 10% bulk water density. An ozone molecule was considered to be adsorbed when the central oxygen was located at a z-position below a somewhat arbitrarily chosen z_{max} value (or above $-z_{max}$ in case of the other interface). The z_{max} value (22 and 24 Å for the 1.2 and 6.1 M solution slabs, respectively) was selected to allow for oscillations of the O_3 z-coordinate occurring when the ozone was adsorbed on the interface (see Figure 3). With this definition, the calculated residence times also include the time when O_3 was, strictly speaking, in the bulk, i.e., located at a z-position corresponding to water density higher than 90% of its bulk value. However, this represents only a minor issue, as the vast majority of such events were limited to 1−2 ps. The maximum time for which O_3 was continuously present in the bulk was of the order of 10 ps, which is more than 1 order of magnitude less than the maximum residence times in/on the interface. In terms of ozone trapping on the surface of the two solutions under study, there was no significant difference in the distributions of O_3 residence times in the interface for the 1.2 and 6.1 M solutions. Both the maximum interface residence times (126 vs 128 ps) and total times during the simulations that O_3 was trapped in the interface (2854 vs 2892 ps) are about the same for the two concentrations. This is in agreement with the findings of a previous study of OH and O_3 interacting with water and two different sodium halide solutions,[92] in which the effect of the dissolved salt on the trapping of the two gas-phase species was small compared to neat water. The propensity of ozone to reside at the interface is likely due to the combination

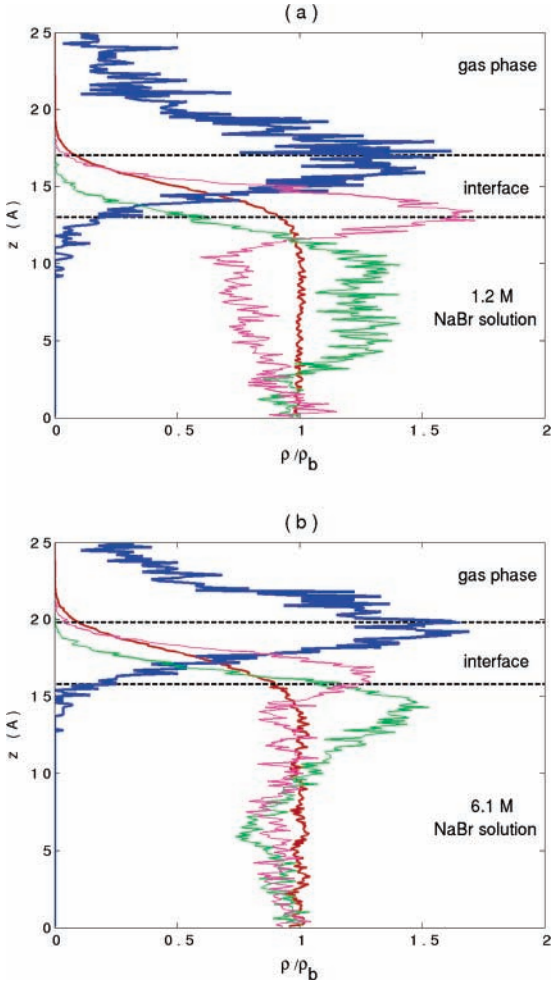

Figure 4. Density profiles obtained from 1-ns simulation of five ozone molecules interacting with (a) 1.2 and (b) 6.1 M NaBr solution. Number densities, $\rho(z)$, of the central O_3 oxygen atoms (blue), water oxygen atoms (red), sodium cations (green), and bromide anions (purple) plotted vs distance from the center of the slabs in the direction normal to the interface (z), normalized by the bulk water density, ρ_b. For ease of comparison, the ion densities were scaled by the water/ion concentration ratio of (a) $n_{wat}/n_{ion} = 48$ and (b) $n_{wat}/n_{ion} = 9$; the O_3 density profiles were scaled by an arbitrarily chosen number n_{scale} (same for both panels).

of its relatively low solubility in water ($H = 1 \times 10^{-2}$ M atm^{-1})[23,98] but significant polarizability (2.85 Å^3). The penalty for perturbing the hydrogen-bonding interactions in bulk water is not compensated by the ozone−water interaction in the bulk liquid. However, at the surface, the water structure is already perturbed and van der Waals interactions between ozone and water at the interface become important.

The density profiles of O_3, together with the density profiles of the water oxygen atoms and the Na^+ and Br^- ions along the z-direction (normal to the surface) for both simulations are shown in Figure 4. The density profiles were averaged over the two approximately equivalent halves of the slab. The interval on the z-axis in Figure 4, in which the water signal decreases from the bulk density value to zero, correlates with the interfacial region of the liquid slab. The dashed horizontal lines correspond to 10% and 90% of water density in the bulk solutions. The O_3 density profiles for the two NaBr solution systems are rather similar. In both cases, the O_3 signal peaks in the outer region of the interface around the 10% bulk water density, and decays rapidly to zero in the bulk, indicating a strong preference of the ozone molecule for partial rather than full solvation.

For both concentrations, the density profiles show evidence of a surface enhancement of Br^- ions accompanied by a spatial separation of the positively and negatively charged ions in the interfacial region, as the Br^- signal peaks and subsequently decays to zero at larger *z*-values compared to the Na^+ signal. The Br^- density profiles in Figure 4a,b exhibit a relatively narrow peak whose maximum coincides roughly with the 90% bulk water density, whereas the substantially wider Na^+ peaks occur well below the interfacial layer. While there are a larger number of bromide ions on the surface of the 6.1 M than the 1.2 M solution as expected, the enhancement of the surface concentration of bromide ions relative to their bulk concentration is less pronounced for the 6.1 M solution compared to the 1.2 M one. This behavior is in contrast to the aqueous NaCl solution where the surface excess of chloride ions appeared to be linear with concentration up to 6.1 M.[115] There are two possible explanations for the observed nonlinear concentration dependence of the surface excess of Br^-: (1) saturation in the build-up of the negative charge on the surface due to the electrostatic repulsion between the ions of the same polarity (the number of Cl^- ions at the surface of the 6.1 M NaCl solution is much less than the number of Br^- ions at the surface of the NaBr solution of the same concentration) or (2) saturation due to steric effects, as only a certain number of ions with their solvation shells can be accommodated on the surface of a given area. In the latter case, the observed difference between the NaBr and NaCl solutions can be related to the different sizes of the bromide and chloride ions. A detailed study of the ionic solvation as a function of concentration, which is outside the scope of this paper, would be required to elucidate this complex issue.

To address the question of the feasibility of the proposed surface mechanism of the ozone reaction with bromide anions, the trajectories were analyzed for the contact between ozone molecules and Br^- ions in the interface. For this purpose, the O_3 (center of mass)$-Br^-$ radial distribution function (RDF) was first calculated, taking into account all configurations for which the O_3 central oxygen was located at a *z*-position smaller than that defined above for the z_{max} value (or larger than $-z_{max}$ for the other interface). The threshold for the O_3-Br^- contact was then set to $r_{cont} = 6.5$ Å, the position of the minimum after the first peak of the RDF, which defines the radius of the first (incomplete) solvation shell around a surface-adsorbed ozone molecule. Rather frequent contacts between O_3 and Br^- are observed. The analysis for the 1.2 and 6.1 M NaBr solutions revealed that the O_3 molecules were in contact with Br^- ions for 27% and 72% of the time that they were adsorbed at the interface, respectively. Typical snapshots from the simulations of both 1.2 and 6.1 M solutions are shown in Figure 5 where the contact between ozone and bromide ions on the surface is evident. The distribution of the contact times is shown in Figure 6. There are a larger total number of O_3-Br^- contact events in the interface of the 6.1 M solution compared to the 1.2 M one, which can be rationalized in terms of more bromide anions being available on the surface of the concentrated solution. In most cases, the O_3-Br^- contact is shorter than 5 ps; however, a substantial fraction of the contact events, in particular for the concentrated NaBr solution, is longer than 10 ps. The increase in the duration of the O_3-Br^- contact for the 6.1 M solution relative to the 1.2 M solution, reflected in both maximum contact times (47 ps vs 26 ps) and mean contact times (6.4 ps vs 3.0 ps), can be largely attributed to enhanced probability of simultaneous contact of ozone with more than one bromide at the surface of the concentrated solution. For the 6.1 M solution,

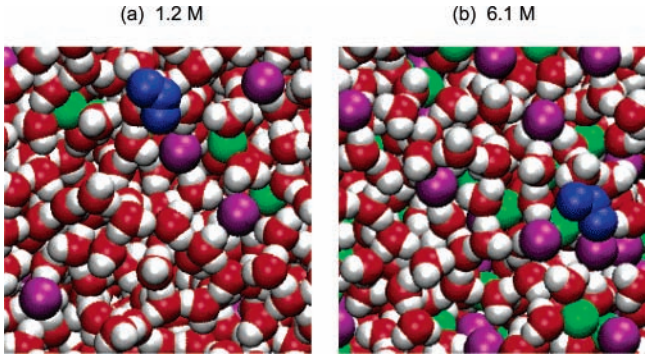

Figure 5. Top view snapshots from MD simulations showing the O_3 molecule in contact with the Br^- ion on the surface of (a) 1.2 and (b) 6.1 M NaBr solution. Color coding: ozone oxygen, blue; bromide anion, purple; sodium cation, green; water oxygen, red; hydrogen, white.

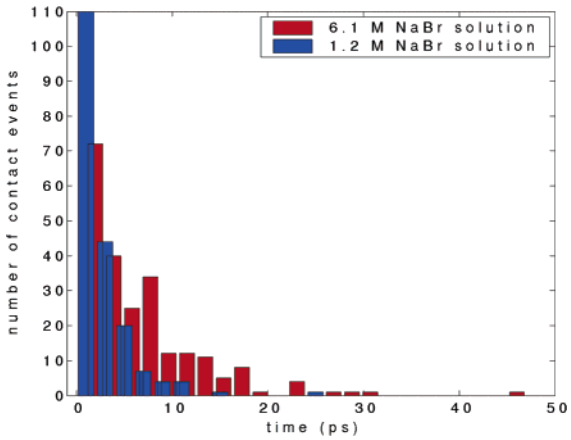

Figure 6. Distribution of contact times between O_3 and Br^- in the interface of 1.2 (blue) and 6.1 M (red) NaBr solutions.

the presence of more than one Br^- ion within r_{cont} distance from O_3 was observed for about 45% of the total contact time, compared to only 10% of the total contact time for the 1.2 M solution. For 15% of the total contact time on the surface of the 6.1 M solution, there were more than two Br^- ions in the vicinity of ozone; such a situation has not been detected for the 1.2 M solution.

Clearly, these results indicate that ozone strongly prefers to reside at the surface of the solution, rather than being taken up into the bulk liquid. Moreover, ozone does come in close contact with Br^-, when adsorbed on the solution surface. Increased salt concentration results in larger frequency of O_3-Br^- contacts as well as longer contact times. Most contacts are limited to just a few picoseconds; however, a nonnegligible fraction of the contacts is longer than 10 ps, with the maximum of almost 50 ps for the 6.1 M solution. The large propensity of ozone for the air$-$solution interface along with the frequent O_3-Br^- contacts observed during the MD simulations indicate that an interface reaction between O_3 and Br^- is feasible.

3.3. Kinetics Modeling Including an Interface Reaction. On the basis of previous work[104,105] and the results of the current MD simulations, it seems likely that the generation of the additional Br_2 observed is initiated by a reaction of O_3 with a bromide ion at the aerosol surface. Several mechanisms for this reaction can be postulated with the first step being formation of the $[O_3\cdots Br^-]$ complex on the surface, reaction R7. After reacting with an additional bromide ion to generate Br_2^-, reaction R8, or an electron transfer to generate atomic bromine, reaction R9, there are several pathways within the interface

TABLE 8: Model Parameters for Modeled Experiments

parameter	units	base case	base case	base case	base case	less aerosol	less aerosol
aerosol:[a]							
median diameter	nm	207	254	272	285	228	222
number concentration[b]	number cm^{-3}	2.40×10^5	3.03×10^5	2.21×10^5	2.92×10^5	1.65×10^5	9.23×10^4
relative humidity	%	68	65	67	67	71	63
$[O_3]_0$	ppm	1.47	1.56	1.65	1.55	1.54	1.53
$\gamma_{\text{surface rxn}}$		2.5×10^{-6}	7.0×10^{-7}	2.7×10^{-6}	2.8×10^{-6}	1.6×10^{-6}	2.6×10^{-6}

parameter	units	high RH	high RH	less O_3	less O_3	larger aerosol	larger aerosol
aerosol:[a]							
median diameter	nm	299	311	314	306	883	842
number concentration[b]	number cm^{-3}	3.13×10^5	2.47×10^5	2.56×10^5	2.40×10^5	9.93×10^3	1.97×10^4
relative humidity	%	87	85	66	64	70	66
$[O_3]_0$	ppm	1.45	1.54	0.34	0.35	1.57	1.61
$\gamma_{\text{surface rxn}}$		9.0×10^{-7}	1.6×10^{-6}	1.0×10^{-6}	1.5×10^{-6}	2.6×10^{-6}	2.4×10^{-6}

[a] Aerosol data are an average of measurements taken at the beginning and end of each experiment. [b] Number concentration given is the number of particles with the median diameter needed to reproduce the total aerosol volume. Data from aerosol measurements were fit to a log-normal distribution and integrated to include aerosol outside the size range of the instruments.

region or the bulk aqueous phase (see Table 4) that can lead to Br_2 formation.

$$O_{3(g)} + Br^-_{(interface)} \rightarrow [O_3 \cdots Br^-]_{(interface)} \quad \text{(R7)}$$

$$[O_3 \cdots Br^-]_{(interface)} + Br^-_{(interface)} \rightarrow O_3^-{}_{(aqueous)} + Br_2^-{}_{(interface)} \quad \text{(R8)}$$

$$[O_3 \cdots Br^-]_{(interface)} \rightarrow O_3^-{}_{(aqueous)} + Br_{(interface)} \quad \text{(R9)}$$

Additional mechanisms were considered, including pathways in which the $[O_3 \cdots Br^-]$ complex leads to oxidation of the bromide to produce BrO^- in the interfacial region. Although the details of the actual mechanism cannot be elucidated by the current analysis, all pathways lead to an overall surface-mediated reaction producing Br_2 in the gas phase and the ozonide radical ion (O_3^-) in the aqueous phase. The O_3^- produced in solution will quickly react with nearby water molecules to produce OH^-, O_2, and OH radical. Because the mechanistic details of the overall process are not known but do result in production of gas-phase Br_2, the net reaction is represented in MAGIC by reaction R10:

$$O_{3(g)} + Br^-_{(interface)} \rightarrow O_3^-{}_{(aqueous)} + {}^1/_2 Br_{2(g)} \quad \text{(R10)}$$

This interface reaction is included in MAGIC with a rate given by

$$R_{\text{interface}} = \gamma_s \frac{\bar{c}}{4} A [O_3]_g \quad \text{(E3)}$$

where γ_s is the probability of the net reaction, R10, occurring for each collision of an O_3 molecule with the droplet surface, $\bar{c}$ is the mean molecular speed, and A is the total particle surface area. This treatment assumes that gas-phase diffusion is not limiting, which is the case in these experiments.[116] It also assumes that the bromide ion concentration at the surface remains approximately constant; in these experiments, the range of bulk aqueous phase bromide ion concentrations varied by ~50%, and the interface concentration would be expected to vary even less due to the preference of bromide ions for the interface.

Data from the modeled experiments were fit by adjusting the value of γ_s to provide a best fit to the experiments. Figure 7 shows the bromine and ozone data for the five representative experiments and the model fits obtained by including reaction R10 of O_3 with Br^- at the interface. It is observed that, given the experimental challenges and uncertainties, a reasonable fit to the Br_2 data is obtained by including the interface reaction. Including the interface reaction also improves the agreement of the ozone data. The best fit values of γ_s for all 12 experiments are listed in Tables 7 and 8. The average for all 12 modeled experiments is $\gamma_s = [1.9 \pm 0.8] \times 10^{-6}$ (1 s). While this value of the reaction probability is small in terms of its absolute magnitude, inclusion of such a reaction is necessary to model the observed data.

Some heterogeneous reactions are best represented by a Langmuir−Hinshelwood mechanism, where a gas-phase species, which is adsorbing and desorbing on/from a surface, reacts with some other surface species.[117] This has been incorporated recently into a resistor model for the analysis of data from laboratory experiments.[118] Since the MD simulations show that ozone readily adsorbs and desorbs to/from the surface, it is reasonable to consider this mechanism. However, such analysis requires experiments over a larger range of concentrations for the gas-phase reactant than was possible in these studies; the range of ozone concentrations used was limited because higher O_3 concentrations significantly changed the API-MS Br_2 calibration, while at lower concentrations the reaction is so slow that bromine production from reactions on the chamber walls becomes more important. It is noteworthy that the best fit reaction probabilities derived for the experiments with ozone concentrations a factor of 4 lower than the base case fall well within the scatter represented by the entire data set. This is in agreement with the results of Anastasio and Mozurkewich,[41] who reported no dependence of the bromine production rate on the ozone concentrations over a range of 30−1000 ppb. Measured reaction probabilities will be independent of the ozone concentration in the case of a Langmuir−Hinshelwood mechanism when the surface is saturated with ozone, so that the reaction rate is determined by the rate constant for the reaction of ozone on the surface with bromide ions.

In an investigation of uptake of ozone by NaI solutions, Hu et al.[74] reported that they did not see evidence of an interfacial reaction between ozone and iodide ion over a range of NaI concentrations of 0.5 to 3.0 M. Their conclusion is based on the linearity of a plot of $1/\gamma$ versus $1/a_{[I^-]}^{1/2}$. However, in similar experiments, they do report occurrence of an interface reaction between Cl_2 and Br_2 with Br^- and Cl^-. It might be expected that if an interface reaction is indeed occurring between ozone and Br^-, it should also occur for I^-, as both of these reactions

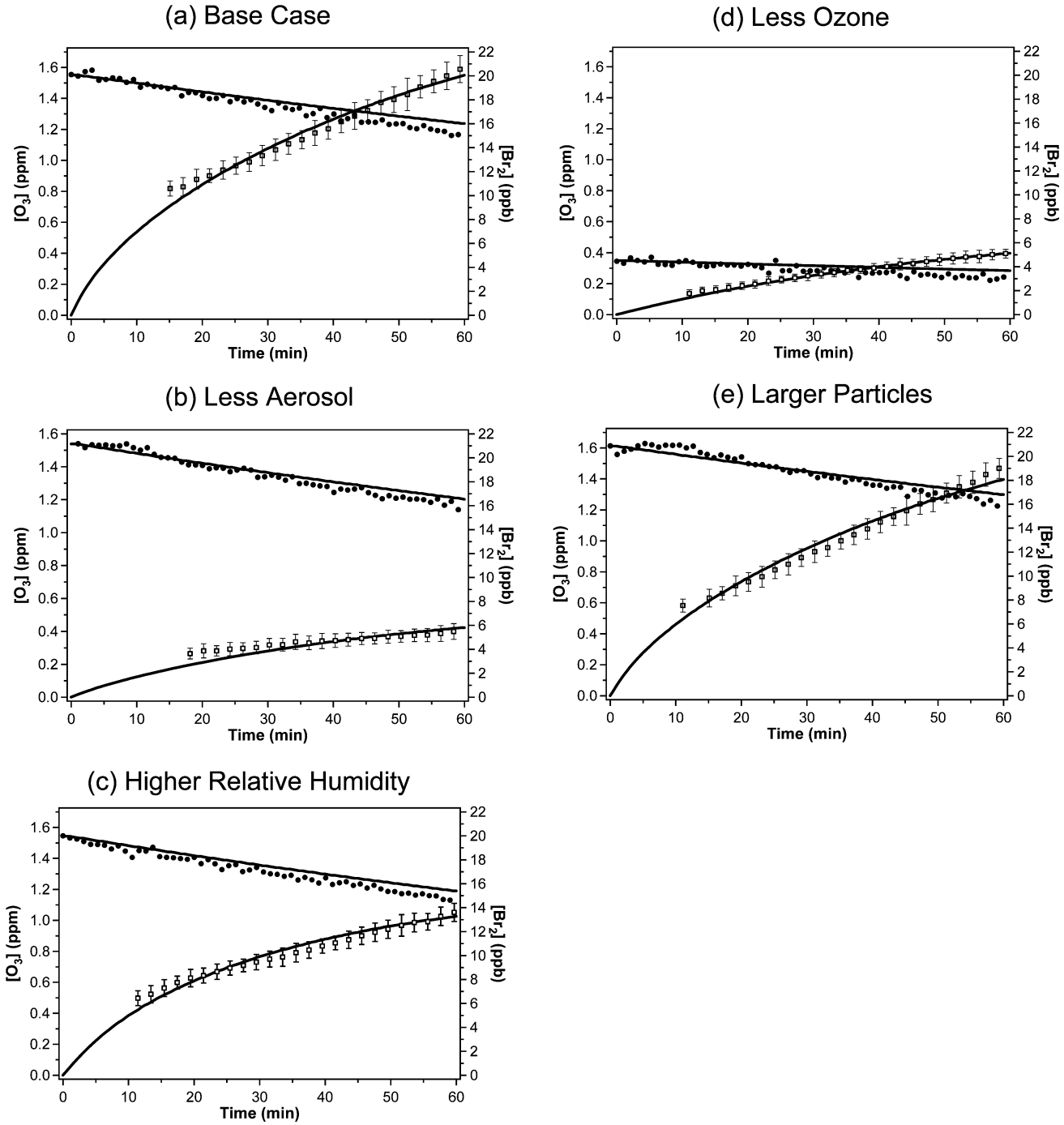

Figure 7. Reaction−time profiles for O_3 and Br_2 in the representative experiments shown in Figure 1. Filled circles and open squares denote experimental ozone and bromine concentrations, respectively. Solid lines indicate the concentrations predicted with MAGIC, including the interface reaction with the reaction probabilities given in Table 7.

occur via an oxygen atom transfer with an $XOOO^-$ intermediate. However, the reaction of O_3 with I^- in the bulk aqueous phase is 7 orders of magnitude faster than its reaction with Br^-,[42] and with this rapid aqueous phase reaction rate, the importance of an interface reaction may be negligible. In addition, the size of the particles in our experiments is much smaller than those in the falling droplet apparatus in which the O_3−I^- studies were performed, and the associated larger S/V ratio tends to favor surface processes relative to those in the bulk.

In their investigation of the reaction of Br^- with O_3 using a flow reactor system, Anastasio and Mozurkewich[41] concluded that additional Br_2 was formed from a reaction of the bromine deposited on the walls of their reaction chamber. Although they propose an enhanced reaction on the glass surface of the reaction chamber, an interface reaction on the aerosol particles could also contribute to the increased bromine production in their system.

4. Atmospheric Implications

On the basis of these experiments, it is likely that molecular bromine will be generated in the marine boundary layer from the reaction with O_3, both in the bulk aqueous phase and by the interface reaction. For a marine environment with 60 ppb ozone and a sea salt particle concentration of 10 cm^{-3} air with a typical diameter of 2 μm, the rate of ozone collisions with the particle surface is 1.7×10^{10} s^{-1} per cm^3 air.[119−124] With a probability of 2×10^{-6} that each collision will produce 0.5

Br_2 molecules, the rate of bromine production is 1.5×10^4 s^{-1} per cm^3 of air. This assumes that the reaction probability measured here for pure NaBr particles is applicable to sea salt. However, it is likely to be an upper limit, since freshly generated sea salt particles have a bromide ion concentration of ~0.8 mM,[23] about 3 orders of magnitude more dilute than the 4.3 to 6.6 M NaBr aerosol particles in these experiments. In the other extreme, where the reaction probability scales with the bulk bromide ion concentration, the production of Br_2 would be ~2 s^{-1} per cm^{-3} of air. However, this will be a lower limit for several reasons. First, MD simulations show that bromide ions prefer to reside at the interface, and in simulations of mixed NaCl/NaBr solutions, bromide has a greater propensity for the surface than chloride.[88] Therefore, although the total number of bromide ions in solution is small, these few ions are likely to be present at the droplet surface frequently and to be available for reaction. Second, in the case of a Langmuir−Hinshelwood type of mechanism, the ozone may reside on the surface and be mobile for sufficient times that it has an increased probability of encountering a bromide ion during this time compared to a hard-sphere collision with the surface; this is supported by the MD simulations discussed above in which ozone molecules are found to be in contact with bromide ions for a large portion of the time they are at the interface. Such a Langmuir−Hinshelwood mechanism will therefore also enhance the rate of production of Br_2 compared to the linear extrapolation of the bulk bromide ion concentration.

Bromine production from the interface reaction can be compared to the rate of production from the aqueous phase oxidation. For the same scenario of particle concentrations and size, and using a rate constant[42] for the O_3-Br^- aqueous phase reaction of 258 M^{-1} s^{-1}, the rate of Br_2 production would be 3 s^{-1} per cm^{-3} of air, comparable to the lower limit for the interface reaction and about 4 orders of magnitude smaller than the upper limit. This treatment assumes that the formation of a $[O_3\cdots Br^-]$ surface complex will result in the formation of Br_2; however, since genuine sea salt contains high concentrations of chloride ions, production of BrCl will likely be more favorable. Since BrCl can photolyze to produce bromine radicals or react with additional Br^- to yield Br_2, the contribution of this surface chemistry on the concentrations of photolyzable halogen species is still expected to be significant.

In short, the reaction of ozone with bromide at the interface of sea salt particles should at least be competitive with the chemistry in the bulk aqueous phase and may be much greater. In 10 h of darkness during the night, a total of 0.003−22 ppt of Br_2 could be produced from this interface chemistry. Measurements of Br_2 have not yet been reported in the marine boundary layer in mid-latitudes, although there is some evidence that it is present at concentrations of ~1 ppt at night.[125] Further laboratory, field, and modeling studies are needed to determine the concentrations of Br_2 in the mid-latitude marine boundary layer and the contribution of this interface chemistry to its formation.

Acknowledgment. This work was supported by the Department of Energy (Grant No. ER 62578) and the National Science Foundation (Grant Nos. 0209719 and 0431512). M.R. was partially supported by a NATO Science Fellowship. We are also grateful to Jorg Meyer for technical assistance and Katherine Thompson for assistance with some of the initial experiments.

Note Added after ASAP Publication. This article was inadvertently released ASAP on 11/26/2004 without several corrections being made. The correct version was posted on 12/07/2004.

References and Notes

(1) Sander, R.; Keene, W. C.; Pszenny, A. A. P.; Arimoto, R.; Ayers, G. P.; Baboukas, E.; Cainey, J. M.; Crutzen, P. J.; Duce, R. A.; Hönninger, G.; Huebert, B. J.; Maenhaut, W.; Mihalopoulos, N.; Turekian, V. C.; Van Dingenen, R. *Atmos. Chem. Phys.* **2003**, *3*, 1301.

(2) Barrie, L. A.; Bottenheim, J. W.; Schnell, R. C.; Crutzen, P. J.; Rasmussen, R. A. *Nature* **1988**, *334*, 138.

(3) Platt, U.; Hausmann, M. *Res. Chem. Intermed.* **1994**, *20*, 557.

(4) Impey, G. A.; Mihele, C. M.; Anlauf, K. G.; Barrie, L. A.; Hastie, D. R.; Shepson, P. B. *J Atmos. Chem.* **1999**, *34*, 21.

(5) Impey, G. A.; Shepson, P. B.; Hastie, D. R.; Barrie, L. A.; Anlauf, K. G. *J. Geophys. Res.* **1997**, *102*, 16005.

(6) Foster, K. L.; Plastridge, R. A.; Bottenheim, J. W.; Shepson, P. B.; Finlayson-Pitts, B. J.; Spicer, C. W. *Science* **2001**, *291*, 471.

(7) Spicer, C. W.; Plastridge, R. A.; Foster, K. L.; Finlayson-Pitts, B. J.; Bottenheim, J. W.; Grannas, A. M.; Shepson, P. B. *Atmos. Environ.* **2002**, *36*, 2721.

(8) Lu, J. Y.; Schroeder, W. H.; Barrie, L. A.; Steffen, A.; Welch, H. E.; Martin, K.; Lockhart, L.; Hunt, R. V.; Boila, G.; Richter, A. *Geophys. Res. Lett.* **2001**, *28*, 3219.

(9) Lindberg, S. E.; Brooks, S.; Lin, C. J.; Scott, K. J.; Landis, M. S.; Stevens, R. K.; Goodsite, M.; Richter, A. *Environ. Sci. Technol.* **2002**, *36*, 1245.

(10) Ebinghaus, R.; Kock, H. H.; Temme, C.; Einax, J. W.; Lowe, A. G.; Richter, A.; Burrows, J. P.; Schroeder, W. H. *Environ. Sci. Technol.* **2002**, *36*, 1238.

(11) Ariya, P. A.; Khalizov, A.; Gidas, A. *J. Phys. Chem. A* **2002**, *106*, 7310.

(12) Ariya, P. A.; Ryzhkov, A. *J. Phys.* **2003**, *107*, 57.

(13) Calvert, J. G.; Lindberg, S. E. *Atmos. Environ.* **2003**, *37*, 4467.

(14) Hönninger, G.; Leser, H.; Sebastian, O.; Platt, U. *Geophys. Res. Lett.* **2004**, *31*, L04111 DOI: 10.1029/2003GL018982.

(15) Skov, H.; Christensen, J. H.; Goodsite, M. E.; Heidam, N. Z.; Jensen, B.; Wahlin, P.; Geernaert, G. *Environ. Sci. Technol.* **2004**, *38*, 2373.

(16) Wang, Z.; Pehkonen, S. O. *Atmos. Environ.* **2004**, *38*, 3675.

(17) Galbally, I. E.; Bentley, S. T.; Meyer, C. P. *Geophys. Res. Lett.* **2000**, *27*, 3841.

(18) Dickerson, R. R.; Rhoads, K. P.; Carsey, T. P.; Oltmans, S. J.; Burrows, J. P.; Crutzen, P. J. *J. Geophys. Res. Atmos.* **1999**, *104*, 21385.

(19) Nagao, I.; Matsumoto, K.; Tanaka, H. *Geophys. Res. Lett.* **1999**, *26*, 3377.

(20) Matveev, V.; Peleg, M.; Rosen, D.; Tov-Alper, D. S.; Hebestreit, K.; Stutz, J.; Platt, U.; Blake, D.; Luria, M. *J. Geophys. Res.* **2001**, *106*, 10375.

(21) Stutz, J.; Ackermann, R.; Fast, J. D.; Barrie, L. *Geophys. Res. Lett.* **2002**, *29*, DOI: 10.1029/2002GL014812.

(22) Friess, U.; Hollwedel, J.; König-Langlo, G.; Wagner, T.; Platt, U. *J. Geophys. Res.* **2004**, *109*, DOI 10.1029/2003JD004133.

(23) Finlayson-Pitts, B. J.; Pitts, J. N., Jr. *Chemistry of the Upper and Lower Atmosphere—Theory, Experiments, and Applications*; Academic Press: San Diego, CA, 2000.

(24) Finlayson-Pitts, B. J.; Livingston, F. E.; Berko, H. N. *Nature* **1990**, *343*, 622.

(25) Finlayson-Pitts, B. J.; Pitts, J. N., Jr. *Science* **1997**, *276*, 1045.

(26) Andreae, M. O.; Crutzen, P. J. *Science* **1997**, *276*, 1052.

(27) Ravishankara, A. R. *Science* **1997**, *276*, 1058.

(28) Finlayson-Pitts, B. J.; Hemminger, J. C. *J. Phys. Chem. A* **2000**, *104*, 11463.

(29) Finlayson-Pitts, B. J. *Chem. Rev.* **2003**, *103*, 4801.

(30) Rossi, M. J. *Chem. Rev.* **2003**, *103*, 4823.

(31) Rankin, A. M.; Auld, V.; Wolff, E. W. *Geophys. Res. Lett.* **2000**, *27*, 3469.

(32) Rankin, A. M.; Wolff, E. W.; Martin, S. *J. Geophys. Res.* **2002**, *107*, art. no. 4683.

(33) Mozurkewich, M. *J. Geophys. Res* **1995**, *100*, 14199.

(34) Behnke, W.; Scheer, V.; Zetzsch. *J. Aerosol Sci.* **1994**, *25*, S277.

(35) Sander, R.; Crutzen, P. J. *J. Geophys. Res* **1996**, *101*, 9121.

(36) Rudich, Y.; Talukdar, R. K.; Ravishankara, A. R. *J. Geophys. Res.* **1998**, *103*, 16133.

(37) Mamou, A.; Rabani, J.; Behar, D. *J. Phys. Chem.* **1977**, *81*, 1447.

(38) Oum, K. W.; Lakin, M. J.; Finlayson-Pitts, B. J. *Geophys. Res. Lett.* **1998**, *25*, 3923.

(39) Hirokawa, J.; Onaka, K.; Kajii, Y.; Akimoto, H. *Geophys. Res. Lett.* **1998**, *25*, 2449.

(40) De Haan, D. O.; Brauers, T.; Oum, K.; Stutz, J.; Nordmeyer, T.; Finlayson-Pitts, B. J. *Int. Rev. Phys. Chem.* **1999**, *18*, 343.

(41) Anastasio, C.; Mozurkewich, M. *J. Atmos. Chem.* **2002**, *41*, 135.

(42) Liu, Q.; Schurter, L. M.; Muller, C. E.; Aloisio, S.; Francisco, J. S.; Margerum, D. W. *Inorg. Chem.* **2001**, *40*, 4436.

(43) Haag, W. R.; Hoigne, J. *Environ. Sci. Technol.* **1983**, *17*, 261.

(44) Sutton, H. C.; Downes, M. T. *J. Chem. Soc. Farady Trans.* **1972**, *68*, 1498.

(45) Buxton, G. V.; Dainton, F. S. *Proc. R. Soc. London Ser. A* **1968**, *304*, 427.
(46) von Gunten, U.; Oliveras, Y. *Environ. Sci. Technol.* **1998**, *32*, 63.
(47) Hoigne, J. *Ozone*: *Sci. Eng.* **1994**, *16*, 113.
(48) Hoigne, J.; Bader, H. *Ozone*: *Sci . Eng.* **1994**, *16*, 121.
(49) Knipping, E. M.; Dabdub, D. *J. Geophys. Res.* **2002**, *107*, 4360.
(50) Schwartz, S. E. Mass-Transport Considerations Pertinent to Aqueous Phase Reactions of Gases in Liquid−Water Clouds. In *Chemistry of Multiphase Atmospheric Systems*; NATO ASI Ser., Vol. G6; Jaeschke, W., Ed.; Springer-Verlag: New York, 1986.
(51) DeMore, W. B.; Sander, S. P.; Golden, D. M.; Hampson, R. F.; Kurylo, M. J.; Howard, C. J.; Ravishankara, A. R.; Kolb, C. E.; Molina, M. J. *Chemical Kinetics and Photochemical Data for Use in Stratospheric Modeling*; National Aeronautics and Space Administration, Jet Propulsion Laboratory, California Institute of Technology: Pasadena, CA, 1997; Evaluation No. 12.
(52) Atkinson, R.; Baulch, D. L.; Cox, R. A.; Hampson, R. F.; Kerr, J. A.; Rossi, M. J.; Troe, J. *J. Phys. Chem. Ref. Data* **2000**, *29*, 167.
(53) Ruasse, M. F.; Aubard, J.; Galland, B.; Adenier, A. *J. Phys. Chem.* **1986**, *90*, 4382.
(54) Beckwith, R. C.; Wang, T. X.; Margerum, D. W. *Inorg. Chem.* **1996**, *35*, 995.
(55) Troy, R. C.; Margerum, D. W. *Inorg. Chem.* **1991**, *30*, 3538.
(56) Taube, H. *J. Am. Chem. Soc.* **1942**, *64*, 2468
(57) von Gunten, U.; Oliveras, Y. *Water Res.* **1997**, *31*, 900.
(58) Kumar, K.; Margerum, D. W. *Inorg. Chem.* **1987**, *26*, 2706.
(59) Beckwith, R. C.; Margerum, D. W. *Inorg. Chem.* **1997**, *36*, 3754.
(60) Faria, R. D.; Epstein, I. R.; Kustin, K. *J. Phys. Chem.* **1994**, *98*, 1363.
(61) Amichai, O.; Treinin, A. *Chem. Phys. Lett.* **1969**, *3*, 611
(62) Kläning, U. K.; Sehested, K.; Wolff, T. *J. Chem. Soc., Farady Trans. 1* **1984**, *80*, 2969.
(63) Zehavi, D.; Rabani, J. *J. Phys. Chem.* **1972**, *76*, 312.
(64) Lind, J.; Shen, X. H.; Eriksen, T. E.; Merenyi, G.; Eberson, L. *J. Am. Chem. Soc.* **1991**, *113*, 4629.
(65) Kläning, U. K.; Wolff, T. *Ber. Bunsen. Phys. Chem.* **1985**, *89*, 243.
(66) Merenyi, G.; Lind, J. *J. Am. Chem. Soc.* **1994**, *116*, 7872.
(67) Ferraudi, G. *J. Phys. Chem.* **1993**, *97*, 2793.
(68) Field, R. J.; Raghavan, N. V.; Brummer, J. G. *J. Phys. Chem.* **1982**, *86*, 2443.
(69) Kläning, U. K.; Olsen, K. J.; Appelman, E. H. *J. Chem. Soc., Farady Trans. 1* **1975**, *71*, 473.
(70) Sutton, H. C.; Boag, J. W.; Michael, B. D. In *Pulse Radiolysis*; Ebert, M., Keene, J. P., Swallow, A. J., Eds.; Academic Press: London, UK, 1965; p 61.
(71) Schwarz, H. A.; Bielski, B. H. J. *J. Phys. Chem.* **1986**, *90*, 1445.
(72) Amichai, O.; Czapski, G.; Treinin, A. *Isr. J. Chem.* **1969**, *7*, 351.
(73) Bartlett, W. P.; Margerum, D. W. *Environ. Sci. Technol.* **1999**, *33*, 3410.
(74) Hu, J. H.; Shi, Q.; Davidovits, P.; Worsnop, D. R.; Zahniser, M. S.; Kolb, C. E. *J. Phys. Chem.* **1995**, *99*, 8768.
(75) Brimblecombe, P.; Clegg, S. L. *J. Atmos. Chem.* **1988**, *7*, 1.
(76) Brimblecombe, P.; Clegg, S. L. *J. Atmos. Chem.* **1989**, *8*, 95.
(77) Schweitzer, F.; Mirabel, P.; George, C. *J. Phys. Chem. A* **2000**, *104*, 72.
(78) Blatchley, E. R.; Johnson, R. W.; Alleman, J. E.; McCoy, W. F. *Water Res.* **1992**, *26*, 99.
(79) Wachsmuth, M.; Gäggeler, H. W.; von Glasow, R.; Ammann, M. *Atmos. Chem. Phys.* **2002**, *2*, 121.
(80) Bell, R. P. *The Proton in Chemistry*, 2nd ed.; Cornell University Press: Ithaca, NY, 1973.
(81) National Institute of Standards, NDRL/NIST Solution Kinetics Database; http://kinetics.nist.gov/solution/, 2004.
(82) Cohen, M. D.; Flagan, R. C.; Seinfeld, J. H. *J. Phys. Chem.* **1987**, *91*, 4563.
(83) Carper, J. *The CRC Handbook of Chemistry and Physics*; Chemical Rubber Publishing Co.: Boca Raton, FL, 1999; Vol. 124.
(84) Case, D. A.; Pearlman, D. A.; Caldwell, J.; Cheatham, T. E. I.; Ross, W. R.; Simmerling, C. L.; Darden, T. A.; Merz, K. M.; Stanton, R. V.; Cheng, A. L.; Vincent, J. J.; Crowley, M.; Tsui, V.; Radmer, R. J.; Duan, Y.; Pitera, J.; Massova, I.; Seibel, G. L.; Singh, U. C.; Weiner, P. K.; Kollman, P. A. *AMBER 6*; University of California, San Francisco: San Francisco, CA, 1999; AMBER 6 was used for generating trajectories.
(85) Berendsen, H. J. C.; Postma, J. P. M.; van Gunsteren, W. F.; DiNola, A.; Haak, J. R. *J. Chem. Phys.* **1984**, *81*, 3684.
(86) Ryckaert, J. P.; Ciccotti, G.; Berendsen, H. C. *J. Comput. Chem.* **1977**, *23*, 327.
(87) Essmann, U.; Perera, L.; Berkowitz, M. L.; Darden, T.; Lee, H.; Pedersen, L. G. *J. Chem. Phys.* **1995**, *103*, 8577.
(88) Jungwirth, P.; Tobias, D. J. *J. Phys. Chem. B* **2002**, *106*, 6361.
(89) Caldwell, J. W.; Kollman, P. A. *J. Phys. Chem.* **1995**, *99*, 6208.
(90) Frisch, M. J.; Trucks, G. W.; Schlegel, H. B.; Scuseria, G. E.; Robb, M. A.; Cheeseman, J. R.; Zakrzewski, V. G.; Montgomery, J. A.; Stratmann, R. E.; Burant, J. C.; Dapprich, S.; Millam, J. M.; Daniels, A. D.; Kudin, K. N.; Strain, M. C.; Farkas, O.; Tomasi, J.; Barone, V.; Cossi, M.; Cammi, R.; Mennucci, B.; Pomelli, C.; Adamo, C.; Clifford, S.; Ochterski, J.; Petersson, G. A.; Ayala, P. Y.; Cui, Q.; Morokuma, K.; Malick, D. K.; Rabuck, A. D.; Raghavachari, K.; Foresman, J. B.; Cioslowski, J.; Ortiz, J. V.; Stefanov, B. B.; Liu, G.; Liashenko, A.; Piskorz, P.; Komaromi, I.; Gomperts, R.; Martin, R. L.; Fox, D. J.; Keith, T.; Al-Laham, M. A.; Peng, C. Y.; Nanayakkara, A.; Gonzalez, C.; Challacombe, M.; Gill, P. M. W.; Johnson, B. G.; Chen, W.; Wong, M. W.; Andres, J. L.; Head-Gordon, M.; Replogle, E. S.; Pople, J. A. *Gaussian 98*, Revision A.11; Gaussian, Inc.: Pittsburgh, PA, 1998.
(91) Maroulis, G. *J. Chem. Phys.* **1999**, *111*, 6846 and references therein.
(92) Roeselová, M.; Jungwirth, P.; Tobias, D. J.; Gerber, R. B. *J. Phys. Chem. B* **2003**, *107*, 12690.
(93) Binding energy of the complex calculated at the MP2/aug-cc-pvdz//CCSD(T)/aug-cc-pvdz level, including the counterpoise correction.
(94) Tachikawa, H.; Abe, S. *Inorg. Chem.* **2003**, *42*, 2188.
(95) Gillies, J. Z.; Gillies, C. V.; Suenram, R. D.; Lovas, F. J.; Schmidt, T.; Cremer, D. *J. Mol. Spectrosc.* **1991**, *146*, 493.
(96) Binding energy of the complex calculated at the MP2/aug-cc-pvdz//CCSD(T)/aug-cc-pvdz level, including the counterpoise correction.
(97) Roeselová, M.; Vieceli, J.; Dang, L. X.; Garrett, B. C.; Tobias, D. J. **2004**, manuscript in preparation.
(98) Sander, R. Compilation of Henry's law constants for inorganic and organic species of potential importance in environmental chemistry, 1999. http://www.mpch-mainz.mpg.de/~sander/res/henry.html (accessed Nov 2004).
(99) Because the small amounts of CO_2 that are present have the potential to modulate the particle pH and hence the chemistry in the bulk of the particles, it is important to incorporate the measured CO_2 into the model appropriately. There is some CO_2 ($0.3-8 \times 10^{14}$ molecules cm^{-3}) in the humid air used, as well as a small increase in CO_2 observed during the experiments. The increase is represented as a rate constant $k(CO_2)_{gen}$, which varied from ($0.3-1.5 \times 10^{11}$) molecules cm^{-3} s^{-1}, and whose value was obtained by varying this rate constant to match the measured CO_2 concentrations. The rate of Br_2 wall loss, represented with a first-order rate constant, $k(Br_2)_{wall\ loss}$, was determined by using the slopes of plots of $\ln([Br_2]_0/[Br_2])$ versus time measured in the separate wall loss experiments as described earlier. As an independent approach, values for $k(Br_2)_{wall\ loss}$ were also obtained by modeling the corresponding wall loss experiments with MAGIC and adjusting the rate to match the data. Values obtained from the first approach were 20−70% larger than those from the kinetics model, since this simple analysis does not account for the dilution of the chamber due to sampling or mass transfer processes. Each model fit value of $k(Br_2)_{wall\ loss}$ was then used in the model of the corresponding ozone experiment.
(100) Hinds, W. C. *Aerosol technology*: *properties, behavior, and measurement of airborne particles*, 2nd ed.; Wiley: New York, 1999.
(101) Disselkamp, R. S.; Chapman, E. G.; Barchet, W. R.; Colson, S. D.; Howd, C. D. *Geophys. Res. Lett.* **1999**, *26*, 2183.
(102) Haruta, K.; Takeyama, T. *J. Phys. Chem.* **1981**, *85*, 2383.
(103) Westerhoff, P.; Song, R. G.; Amy, G.; Minear, R. *J. Am. Water Works Assoc.* **1998**, *90*, 82.
(104) Knipping, E. M.; Lakin, M. J.; Foster, K. L.; Jungwirth, P.; Tobias, D. J.; Gerber, R. B.; Dabdub, D.; Finlayson-Pitts, B. J. *Science* **2000**, *288*, 301.
(105) Laskin, A.; Gaspar, D. J.; Wang, W. H.; Hunt, S. W.; Cowin, J. P.; Colson, S. D.; Finlayson-Pitts, B. J. *Science* **2003**, *301*, 340.
(106) Jayne, J. T.; Davidovits, P.; Worsnop, D. R.; Zahniser, M. S.; Kolb, C. E. *J. Phys. Chem.* **1990**, *94*, 6041.
(107) Hanson, D. R.; Ravishankara, A. R. *J. Phys. Chem.* **1994**, *98*, 5728.
(108) George, C.; Behnke, W.; Scheer, V.; Zetzsch, C.; Magi, L.; Ponche, J. L.; Mirabel, P. *Geophys. Res. Lett.* **1995**, *22*, 1505.
(109) Boniface, J.; Shi, Q.; Li, Y. Q.; Cheung, J. L.; Rattigan, O. V.; Davidovits, P.; Worsnop, D. R.; Jayne, J. T.; Kolb, C. E. *J. Phys. Chem. A* **2000**, *104*, 7502.
(110) Clegg, S. M.; Abbatt, J. P. D. *J. Phys. Chem. A* **2001**, *105*, 6630.
(111) Katrib, Y.; Deiber, G.; Schweitzer, F.; Mirabel, P.; George, C. *J. Aerosol Sci.* **2001**, *32*, 893.
(112) Mmereki, B. T.; Donaldson, D. J. *J. Phys. Chem. A* **2003**, *107*, 11038.
(113) Jungwirth, P.; Tobias, D. J. *J. Phys. Chem. A* **2002**, *106*, 379.
(114) Jungwirth, P.; Tobias, D. J. *J. Phys. Chem. B* **2001**, *105*, 10468.
(115) Jungwirth, P.; Tobias, D. J. *J. Phys. Chem. B* **2000**, *104*, 7702.
(116) The reaction rate taking into account both the collision rate and gas-phase diffusion is given by $R = [r/D_g + 4/(\gamma_s c)]^{-1} A[O_3]$, where r is the particle radius and D_g is the gas-phase diffusion coefficient. For the small value of γ_s determined here (see text), the second term dominates by about 6 orders of magnitude and gas-phase diffusion limitations are not important.
(117) Adamson, A. W. *Physical Chemistry of Surfaces*, 6th ed.; Wiley: New York, 1997.

(118) Ammann, M.; Poschl, U.; Rudich, Y. *Phys. Chem. Chem. Phys.* **2003**, *5*, 351.
(119) Blanchard, D. C. *Ann. N.Y. Acad. Sci.* **1980**, *338*, 330.
(120) Fitzgerald, J. W. *Atmos. Environ.* **1991**, *25A*, 533.
(121) de Leeuw, G.; Neele, F. P.; Hill, M.; Smith, M. H.; Vignati, E. *J. Geophys. Res.* **2000**, *105*, 29397.
(122) Hoppel, W. A.; Frick, G. M.; Fitzgerald, J. W. *J. Geophys. Res.* **2002**, *107*, AAC7.
(123) Maring, H.; Savoie, D. L.; Izaguirre, M. A.; Custals, L.; Reid, J. S. *J. Geophys. Res.* **2003**, *108*, PRD3.
(124) O'Dowd, C. D.; Smith, M. H. *J. Geophys. Res.* **1993**, *98*, 1137.
(125) Spicer, C. W. personal communication, 2004.